RSC Advances

This is an *Accepted Manuscript*, which has been through the Royal Society of Chemistry peer review process and has been accepted for publication.

Accepted Manuscripts are published online shortly after acceptance, before technical editing, formatting and proof reading. Using this free service, authors can make their results available to the community, in citable form, before we publish the edited article. This *Accepted Manuscript* will be replaced by the edited, formatted and paginated article as soon as this is available.

You can find more information about *Accepted Manuscripts* in the Information for Authors.

Please note that technical editing may introduce minor changes to the text and/or graphics, which may alter content. The journal's standard Terms & Conditions and the Ethical guidelines still apply. In no event shall the Royal Society of Chemistry be held responsible for any errors or omissions in this *Accepted Manuscript* or any consequences arising from the use of any information it contains.

ROYAL SOCIETY OF CHEMISTRY

www.rsc.org/advances

Photothermal response of the plasmonic nanoconglomerates in assembled films by electroless plating approach

Milana Lisunova,[1,*] Xingfei Wei,[1,*] Drew DeJarnette,[2] Gregory T. Forcherio,[2] Keith R. Berry,[1] Phillip Blake,[1] D. Keith Roper[1,2,†]

* The two authors contributed equally

[1] Ralph E. Martin Department of Chemical Engineering, 3202 Bell Engineering Center,

[2] MicroElectronics-Photonics Program, Institute for Nanoscience and Engineering, University of Arkansas, Fayetteville, AR 72701

[†] To whom correspondence should be addressed.

Tel: +1 479 575 6691

Fax: +1 479 575 7926

e-mail: dkroper@uark.edu

RSC Advances Accepted Manuscript

Table of contents entry

Conversion of light energy to heat by ordered gold nanostructures on a gold film has been investigated.

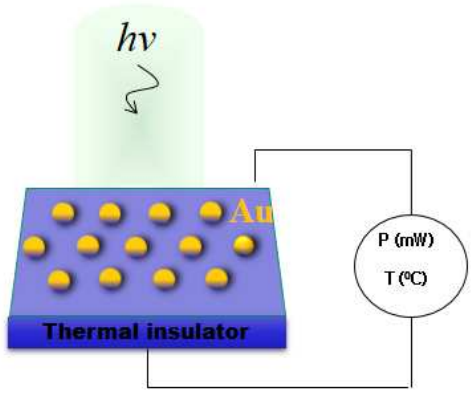

RSC Advances Accepted Manuscript

Abstract

Photothermal transduction of light to heat by evaporated and electroless plated gold (Au) films has been compared. Bare film was compared with film decorated by an ordered lattice of Au nanocylinders. Effects of plasmonic absorption of incident light, heat dissipation in the substrate, and interfacial effects between Au nanoparticles and substrate were evaluated. Differences in the photothermal response of the films emerged due to interactions between these effects. Significant photothermal transduction was achieved by 30-40 nm Au grains as well as by conglomerate nanocylinders assembled from Au grains. An electroless Au film decorated with conglomerate Au nanocylinders ordered into a hexagonal array enhanced attenuation 22% and increased light-to-heat conversion 26%. This was attributed to photon-plasmon coupling. Evaporated Au film of 57 nm thickness attenuated 30% of incident light, compared to 45% attenuation for the electroless film of 35 nm thickness. Evaporated film had a photothermal response of 280^0C per watt of incident light in contrast to 1400^0C per watt for the electroless film.

RSC Advances Accepted Manuscript

Introduction

Two-dimensional (2D) ordered lattices of plasmonic metal nanoparticles (NP) can improve the performance of photovoltaic devices like solar cells, sensors, and energy convertors due to enhanced local electromagnetic fields induced by incident, resonant irradiation.[1,2,3,4,5,6] Ordering plasmonic NP into square lattices of dimers is reported to enhance electric field intensity up to $(|E|^2) > 10^7$.[7,8] Ordered lattices of metals on semiconductor surfaces is reported to increase photocurrent 43% under white-light illumination, compared with 8% increase by disordered NP.[9] A photovoltaic device constructed with a periodic lattice of noble metal NP was recently shown to be operable at room temperatures and without a bias voltage, which increased the efficiency of the device.[10] Adjustments to the lattice constant were recently shown to provide tenability of the extinction spectra. Underlying diffractive modes that support specific adjustments were identified by complex geometry [11] and fully characterized using the coupled dipole approximation.[12] Optical tunability by NP location[13] and orientation also supports use of 2D ordered lattices as platforms for optical sensing [14] or to perform wavelength-selective detection.[15,16,17] Sensitivity in 2D ordered lattices is enhanced relative to single- or random-NP plasmon-based sensing.[18] Tunability provided by polarization of incident irradiation supports consideration of 2D ordered NP lattices as novel light detection systems.[19]

However, dissipative thermal losses from plasmonic absorption in 2D ordered lattices, which impacts cost-effective implementation of lattices in solar photovoltaic or sensor applications, remains relatively unexamined. Quantitative characterization of dissipative absorption in 2D lattices has been constrained by limited availability of lattices of sufficient area to support calorimetric evaluation.[20,21,22] On the other hand, thermoplasmonic transduction has been widely evaluated for random nanoparticles in single-phase fluid suspensions[23] and on solid substrates[24] and at two-phase solid-fluid interfaces. [25] Micro-scale thermoplasmonic systems exhibit predictable thermodynamic and transport behaviors. [26] It has been reported that isolated plasmonic NP are about 97±8 % efficient in converting photon to heat energy.[24] Govorov et al. showed irradiating plasmonic NP at a frequency near resonance can drive the NP through a phase transformation when they are in thermal contact with a polymer or a solid matrix, such as ice. [27 , 28] Plasmonic photothermalization can be so strong as to recrystallize plasmonic nanoparticles, which leads to shape transformation. [29] Vaporization of water[24] and other optofluidic effects coming from heated metal plasmonic nanoparticles has been reported. In particular, embedding NP in flexible biocompatible polymers enhances thermoplasmonic transduction in proportion to nanoparticle concentration. [30] Halas, El'Sayed, and their collaborators showed plasmonic photothermalization was viable for thermal ablation of cancer and bactera.[31,32,33,34,35]

Extrapolation of photothermal effects of isolated NP to ordered lattices of NP has been constrained to date by electrodynamic, electrostatic, and thermal considerations. Govorov et al. [36] predicted that ordering NP into lattices screens the electric field inside the lattice in a way that

RSC Advances Accepted Manuscript

reduces or increases total heat dissipation, depending on the incident light polarization. Emergence of coupling between photons diffracted by the lattice structure and plasmons supported by NP at the nodes is anticipated to enhance photothermal effects at coupling frequencies.[11,12] Conversely, reducing the lattice constant would eliminate coupling but increase dissipative adsorption from lattices with NP at a higher area density. Sixteen plasmonic nanoparticles in a square lattice under incident illumination at 10^4 W/cm^2 produced a temperature increase of 25 K versus 5 K for a single nanoparticle under the same conditions.[36] Beyond these brief evaluations, examination of thermoplasmonics in ordered NP lattices remains limited, despite its significance to dissipative absorption. [37,38]

This work examines the effects of nanostructure on thermoplasmonic transduction in continuous and semi-continuous Au film alone, and in conjunction with 2D ordered lattices of Au NP. Au nanofilms (continuous film and hexagonal array) with similar grainy morphology and dimensions were produced by electroless plating (ELP)[39] onto an electron resist patterned by electron-beam lithography (EBL).[40] The electroless film and film plus NP lattice were lifted off the electron resist and underlying ceramic substrate using adhesive tape.[41] Electroless films were compared with conventional Au nanofilms produced by metal evaporation. The grainy Au morphology resulting from batch ELP increased thermoplasmonic dissipation relative to evaporated films. Nanostructures composed of self-assembled Au grains during electroless deposition exhibited higher absorption, attenuation light-to-heat energy conversion than smooth evaporated films which yield lower thermal responses due to increased optical scattering.

RSC Advances Accepted Manuscript

Results and Discussions

The nanostructure of Au elements films produced by electroless plating varies substantially with processing conditions. In scanning electron microscopy (SEM) images, films produced by batch electroless plating appear to result from coalescence of individual gold islands, compared to Au films formed by continuous-flow electroless plating or evaporation, which have increased continuity.[41] Au grain sizes between 30-40 nm for films produced by electroless plating (ELP) have been reported in several studies. [39,40,41,42,43] In this work, batch electroless plating was used to prepare bare Au film and Au film decorated by ordered Au nanostructures. Fig 1, panels a and b show ELP grainy film (a) and when decorated with conglomerate nanocylinders organized into a hexagonal lattice with a period of 700 nm (b) (see also Fig. S2). The diameter of the conglomerate Au nanocylinders is about 120-160 nm with a wall height of 100-120 nm and a thickness proportional to grain dimensions (see Fig. S2). The grainy electroless Au films nanoclusters result in a porous matrix (see Fig. 1, a and Fig. S3).[39] The overall dimensions of the films were about 5 by 5 mm, which supported evaluation of optical and thermal properties. In contrast to batch ELP, widely-used metal evaporation of Au results in continuous smooth films with low porosity. Fig. 1, panel c shows an SEM of an evaporated Au film 57 nm in height (see also Fig. S4).

Fig. 2 compares transmission UV-vis extinction spectra in air of ELP Au grainy film, ELP grainy film decorated with hexagonal arrays of conglomerate nanocylinders, and evaporated Au film. The two grainy Au films exhibit broad extinction spectra arising from the random distribution of the nanoparticles and porous structure. The spectra from the evaporated Au is similar, albeit with a different slope (500 nm to 850 nm). In contrast to the UV-vis spectra of the undecorated Au films, the film decorated with Au nanocylinders exhibits an additional feature at 547 nm. All the Au films exhibit an extinction minima (transmission peak) at 500 nm. This feature has been attributed to photoluminescence caused by electron transitions and recombination between filled *d*-bands and the Fermi-level conduction band in the Au.[39, 44] Numerous reports indicate photoluminescence is pronounced in Au films with a thickness less than 60 nm. [45,46,47,48,49]

To interpret the transmission spectra, discrete dipole approximation (DDA) of representative nanostructures was performed. First, to evaluate the effect of nanostructure shape on the spectra, a single conglomerate Au nanocylinder and a solid Au nanocylinder were simulated (see Fig. 3) using a shape file generated in Matlab. Both cylinders had a 120 nm outer diameter, 40 nm wall thickness, and were 100 nm in height. The Au dielectric constant for the simulations was taken from Johnson and Christy.[50] The propagation of light was along z direction, parallel to the axis of the nanocylinder. The conglomerate and solid cylinders each displayed two characteristic extinction peaks at 729 nm /564 nm and 702 nm /562 nm, respectively. While the solid cylinder extinction peak consisted of 20% absorption, the conglomerate extinction was comprised of 70% absorption at the plasmon wavelength. Note that percentages were estimated using the area under the curves, not at the peak wavelength. From these results, Au grains with diameter of 40

RSC Advances Accepted Manuscript

nm assembled into a nanocylinder could be expected to produce a higher absorption/scattering yield ratio compared to a solid Au nanocylinder, despite overall similarity across the extinction spectra. This is consistent with the fact that particles larger than 60 nm in radius exhibit primarily scattering behavior under resonant illumination.[51] The nanostructure (shape, aspect ratio) defines the absorption and scattering. For instance, nanoparticles shaped as a hollow cage and a solid rod, despite similar effective radiuses, possess different scattering/absorption yield ratios.[44,52]

Second, to evaluate the effect of decoration by an ordered 2D lattice, the grainy cylinders in a hexagonal array with a period of 700 nm were simulated, as well as Au grains assembled in continuous films. Au grains in a continuous film possess a broad spectra shaped similarly to the experimental spectra (see Fig. 2). The broadening depends on the dimensions of the clusters (assembled grains form a cluster). The experimentally observed spectra could result from a superposition of plasmonic responses from clusters of different sizes. The simulations for both films show an extinction minima close to 500 nm (512 nm for the hexagonal array and 500 nm for the grains assembled in continuous films), which is similar to the experimental spectra (see Fig. 2). However, the hexagonal lattice of cylindrical nanoconglomerates (see Fig. 4) display features that are smoothed in experimentally observed spectra (see Fig. 2). These features may be attributed to the effect of the Au grainy background and the broad shape distribution of cylinders. The defects of the surface[53] also lead to the broadening of the UV-vis spectra.

In order to quantitate geometric optics of the Au nanostructures, a bi-directional spectroscopy apparatus constructed around an integrating sphere[54] was employed to measure reflection (R) and transmission (T) of the thin films. With this apparatus, attenuation (A) could be determined by:

$$A = 1 - T - R \quad (1)$$

Attenuation includes both dissipative plasmonic absorption and bulk non-resonant losses from the sample.[38] As shown in Fig. 1, the plasmonic absorptive nanostructure consists of conglomerate Au metal nanocylinders deposited on top of a gold film which is adhered to the dielectric substrate (Fig. 5). The dielectric substrate was 70 μm thick. It transmitted 92% of incident green light, reflected 1.72%, and had a resulting attenuation of 6%. The dielectric substrate on which 40 nm Au grains were deposited in a film attenuated 45%, while the same substrate and film decorated by grainy conglomerate Au nanocylinders attenuated > 54%. Note that, the estimated volume of grainy film with and without nanocylinders was approximately the same (see Supporting info). The observed differences in attenuation could be due to differences in Au particle morphology or from the addition hexagonal ordered nanostructures. The ordered nanostructures create a potential for far field inter-particle coupling. It is noteworthy that the Au films decorated by conglomerate Au nanocylinders transmit a lower percentage of light (10% less) compared to Au film without the nanocylinders. At the same time, reflection improved slightly from 6.7% to 9.3 % suggesting that nanocylinders scatter light at a comparable level to grainy Au films.

RSC Advances Accepted Manuscript

The effect of nanostructure on optical attenuation was further analyzed using the evaporated Au which produced a smooth film of about 57 nm in height. The attenuation of the Au smooth film was 30%, compared to 45% attenuation by the 35 nm grainy film. Attenuation decreased despite a higher amount of the deposited Au (1.4 fold higher). Recent reports concur that nanostructure impacts optical attenuation. Cai et al. improved reflection properties (reflection <0.5% in the visible region and <2% in the near infrared region) of TiO_2 nanorod arrays by optimizing the graded reflective index profile that results from the hierarchical tips-on-rod structure of the microcrystalline nanorods.[55] Liu et al.[56] improved light attenuation by approximately 30% by designing organized TiO_2 nanoparticles.

ELP Au films with and without Au nanocylinders exhibited a photothermal response to incident green light at a wavelength of 532 nm. Measured temperatures of ELP Au films increased as the power of incident light increased from 0 to 45 mW: from 22 ^{0}C to 62 ^{0}C for Au film alone; and from 22 ^{0}C to 76 ^{0}C for Au film decorated with nanocylinders) (see Fig. 6). The variation is linear for both samples. Higher temperature variation of $\Delta T=54$ ^{0}C for the film decorated with nanocylinders, compared to $\Delta T=40$ ^{0}C for the undecorated Au grainy film was consistent with its higher attenuation level. Higher photothermal response at larger attenuation was previously reported by Roper and coworkers for a 7 μm layer of Au nanoparticles (NP) penetrated into 130 μm thick polydimethylsiloxane (PDMS) films; [57] and for a random distribution of Au nanoparticles in PDMS.[30] Higher attenuation in the latter was coincident with a larger concentration of embedded Au NP.

The photothermal response of the grainy thin films could result from interaction between several factors. The protrusion of the conglomerate nanocylinders from the surface of the grainy film could absorb and transduce more light to heat. Interparticle coupling between scattered photons and plasmon noted in ordered lattices that impacts the electromagnetic field enhancement[12,13,14,16,18,21,24] could also increase photothermal transduction. The low intimate bonding (interfacial contact) of nanocylinders at the surface could reduce measurable heat dissipation. To evaluate the effect of ambient conditions, the top of the Au film was insulated by optically transparent tape. The evaporated Au film shows a negligible thermal response to irradiation under similar conditions (see Fig. 6). The difference in thermal response between the smooth evaporated film and the grainy ELP film appears largely due to the different absorption/scattering cross section of the films. This suggests that the thermal response is not only determined by the mass of deposited Au, but also by interactions arising from the deposited Au nanocylinders as well as the intrinsic nanostructure of each Au film and feature.

The photon-to-heat conversion of the nanocylinder-decorated film and bare grainy film, respectively, were up to 1700 ^{0}C/W and 1400 ^{0}C/W. These are comparable to previously reported values for Au NP embedded in polymer films at significantly lower Au content, about ~ 0.04 vol%. It is noteworthy that reducing Au asymmetrically into thin PDMS increased the photon-to-heat conversion relative to more uniform Au NP reduction by about a factor of two.[57]

RSC Advances Accepted Manuscript

The method used to measure photon-to-heat conversion provides a measure of dissipated heat from the excited nanoparticles to the polymer substrates. There is an emerging interest in distinguishing local temperature variation due to plasmonic excitation of nanoparticles in a lattice. The measurement is precluded by ultra-fast heat dissipation (100-380 ps)[58] from the high thermo-conductive Au plasmonic nanoparticles of about 110 (W/mK) as well as ultra-low time relaxation of about $<10^{-9}$ s. [28,38,59] One study reported plasmonic metamaterials' transient temperature increased about 795 K during an ultrafast photothermal process.[60,61] Improved understanding of photon-to-phonon energy conversion by nanoparticles and heat dissipation to the surrounding environment is a widespread goal. For instance, Zeng and Murphy[62] used a finite element analysis heat transfer model to compare temperature variation of randomly distributed NP over a long duration with short, high-powered pulsed laser heating. The local temperature increased from 300 K to 750 K for NP with a radius of 20 nm and from 300 K to 650 K for NP with radius of 40 nm as the volume fraction of NP increased from 0 to 0.01. Not surprisingly, increasing the gold content improved the temperature increase: local temperature increased from 300 K to 3000 K for NP with radius of 40 nm and from 300 K to 650 K for NP with a radius of 20 nm as the amount of NP per unit volume increase from 0 to 3×10^{7} (nm^{-3}). The study concluded that for a given number of NP per unit volume, the temperature increased as NP size increased, while at constant volume fraction the temperature variation was not affected by NP size. Carlson et al.[63] reported a discontinuous differences between the measured temperature of the substrate and the local temperature of 40 nm Au NP of about 800 K due to interfacial effects (such as effective dielectric constant and the interface conductance) that limit heat transport to the sensor films. Binding of plasmonic NP to the surface was reported to affect the heat flow in the film and measured heat dissipation. Analysis of melting points of metals suggests that plasmonic NP could attain a local temperature of thousands of Kelvin.[64,65] However, measured temperature increases are only on the order of a few tens of degrees due to the difference in the heat capacities as reported by Ashcroft.[66]

It is possible that the higher thermal response of grainy Au films compared with smooth evaporated films could result from electromagnetic field enhancement via coupling of photoluminescent and surface plasmonic modes.[67,68,69,70] Enhancement of electromagnetic field due to coupling between plasmon modes and photoluminescence emission has been reported in in hybrid materials that include Au nanoparticles, such as CdS nanoparticles on the Au films,[66] ZnO deposited on Au nanoparticles,[68] and dye doped by Au nanoparticles.[71] However, the lack of research on photoluminescence coupling with plasmonic modes in non-hybrid Au nanostructures could motivate further work in this area.

In conclusion, this work considered the thermoplasmonic response of conglomerate Au films with and without attendant nanostructures. Effects of heat dissipation in the substrate-tape, energy harvesting and conversion by plasmonic Au nanostructures (absorption versus scattering, transmission/attenuation/reflection), and interfacial effects between Au nanoparticles and

RSC Advances Accepted Manuscript

substrate were considered. The increase in photothermal responses for grainy electroless Au film when decorated with a lattice of conglomerate Au nanocylinders appeared to result from several factors. Films composed of Au grains from 30-40 nm in diameter and nanocylinders assembled from such Au grains absorb a higher percentage of light than smooth evaporated films that results in higher light to heat conversion. The presence of a lattice of conglomerate Au nanocylinders on the grainy Au film increased attenuation 22% and enhanced light to heat conversion by 26%. Weak interfacial bindings of the cylinders, due to porosity of the grain Au substrate, affected the heat flow and allowed an increase in light detection of only 26%.

Overall, an increase in photothermal response of films produced by electroless plating was observed compared with metal evaporated films. Evaporated Au film of 57 nm thickness had less attenuation of 30% compared to grainy film of 35 nm which attenuated 45%, and a lower thermal response of 280^0C/W in contrast to 1400^0C/W for the grainy film.

Experimental part

Sample preparation. The Au films studied were mechanically transferred to the adhesive tape. The grainy arrays were produced via electron beam lithography (EBL) on ITO coated glass substrates and electroless plating (ELP) the preliminary features given by the width of the beam and depth of resistance on the ITO template.[72] First, the clean glass substrate was spin-coated with 150 nm thin film electron-sensitive resist, ZEP 520 (Nippon ZEON Ltd.) diluted 1:2 in methoxybenzene (SI, Fig. 1a). The resolution of the EBL system used (FEI, Hillsboro, OR) is approximately 20 nm, employing an accelerating voltage of 30 kV (SI, Fig. 1b). Patterns were developed in amyl acetate (SI Fig. 1c), creating a patterned resist film. The pattern was Au-plated by successive deposition of tin (SI Fig. 1d), silver (Fig. 1e), and gold (Fig. 1f) in electroless plating solutions. The sacrificial resist was dissolved in acetone (SI Fig. 1 f), and top array was lifted-off by adhesive tape (SI Fig. 1h), producing finally two arrays: one on the tape and another on the ITO substrate, with overall dimensions of 5 mm x 5 mm.

Optical characterization of nanoparticle arrays. Transmission extinction measurements reported here were recorded with an Andor Shamrock 303i spectrometer over the range 350 to 850 nm. The spectrometer was coupled to a Nikon Eclipse LV100 inverted microscope, used to localize light onto the desired sample area. The probing white light was collimated to approximately 50 μm. Transmitted light was beam split into the spectrometer after passing through the microscope.

Attenuation/Transmission/Reflection Far-field optical properties of each sample were characterized using a custom spectroscopy setup built around a polytetrafluoroethylene (PTFE) integrating sphere (IS200-4, Thorlabs, Newton, NJ), previously described by Forcherio et al.[73] Samples were affixed to the exterior of the integrating sphere, and normally irradiated by a circular 532 nm laser (MXLFN-532, CNI, Changchung, CN) 2 mm in diameter. Transmission was recorded with a power meter (PM100D, Thorlabs Newton, NJ, USA) behind the sample,

RSC Advances Accepted Manuscript

with a detection area large enough to capture all transmitted light. Reflected light was captured by the integrating sphere and detected by a fiber-coupled spectrometer (AvaSpec-2048, Avantes, Broomfield, CO, USA). Detected transmission and reflection signals were normalized with respect to a sample-less aperture and PTFE mirror, respectfully. Reported figures of transmission, reflection, and attenuation are an average of three trials (the absolute errors are presented as error bar on Fig. 5 and relative errors are 1-3%)

Thermal properties measurement: Thermal data was captured using 5 mm × 5 mm samples of the films suspended horizontally with the laser spot (1.2 mm diameter) centered within the film. This method was similar to that used in a previous report.[30,57] The samples were deposited by back side to the infrared thermal imaging camera (ICI 7320, Infrared Cameras Inc., Beaumont, TX, USA). The laser power was set to 18 mW to match both the power used in the integrating sphere setup and to keep the infrared camera within its operational temperature range (<100 °C). Laser power was monitored before and after each trial to make sure it remained constant (the variation is within 4% of the measured). The infrared camera recorded the thermal data at 1 Hz during a 3 min heating period with the laser on and a 3 min cool down period with the laser turned off.

Simulations. The discrete dipole approximation (DDA) package DDSCAT method was utilized for simulation.[74,75] The calculations here refer to air as the external dielectric medium. The dispersive gold (Au) dielectric values in all calculations were taken from Johnson and Christy.[76] The shape files of hollow cylinders as well as porous cylinders had been simulated via utilization Matlab. The plasmonic spectra of the cylinders with a specified shape were evaluated via the reading shape file by DDSCAT, specifically by FROM_FILE (geometry read from shape file). Spectra of the agglomerated grains versus the amount of the particles were calculated via the reading shape file by DDSCAT, specifically by SPH_ANI_N (collection of N anisotropic spheres).

Hexagonal arrays of particles were simulated using an infinite coupled dipole approximate (CDA).[11,12,19] Nanoparticles in the CDA were treated as single, point dipoles with specified dipole polarizability as a function of incident wavelength, particle composition and morphology, and surrounding dielectric environment. Polarizability values for the individual nanoparticles were determined by summing constituent polarizabilities using the DDA as described in recent paper.[77] Electric fields from each nanoparticle in the hexagonal array were summed on a center particle to determine extinction efficiency of incident light.

Supporting Information

Supporting Information is available from the Royal Chemical Society or from the author.

Acknowledgements

RSC Advances Accepted Manuscript

This work was supported in part by NSF ECCS-1006927, NSF CBET 1134222, the University of Arkansas Foundation, and the Walton Family Charitable Support Foundation. Any opinions, findings, and conclusions or recommendations expressed in this material are those of the authors and do not necessarily reflect the views of the National Science Foundation. The Arkansas Bio Nano Materials Characterization Facility is supported in part by the NSF.

RSC Advances Accepted Manuscript

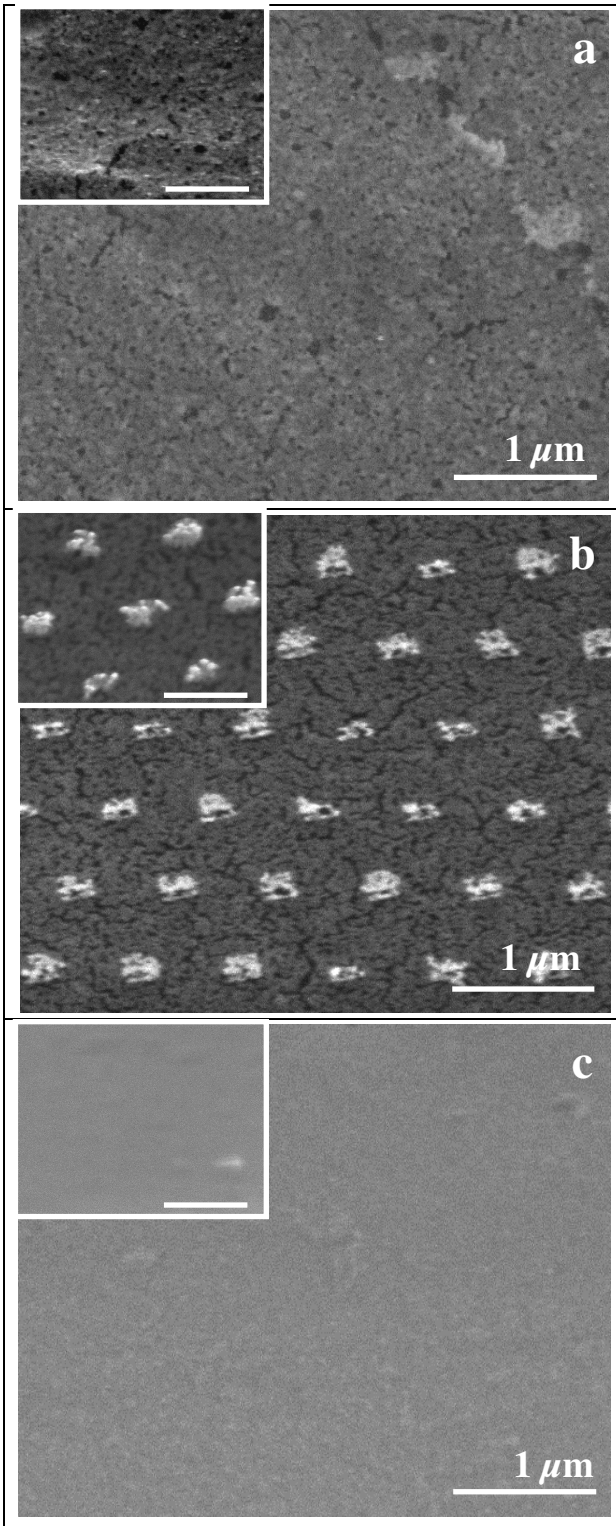

Fig. 1 SEM images of Au grainy film (a) and hexagonal array of the Au cylinder-nanoconglomerates on the Au grainy film (background) (b). SEM image of Au evaporated film (c). Insets are SEM images tilted to 45°. The scale bar in the insets corresponds to 500 nm.

RSC Advances Accepted Manuscript

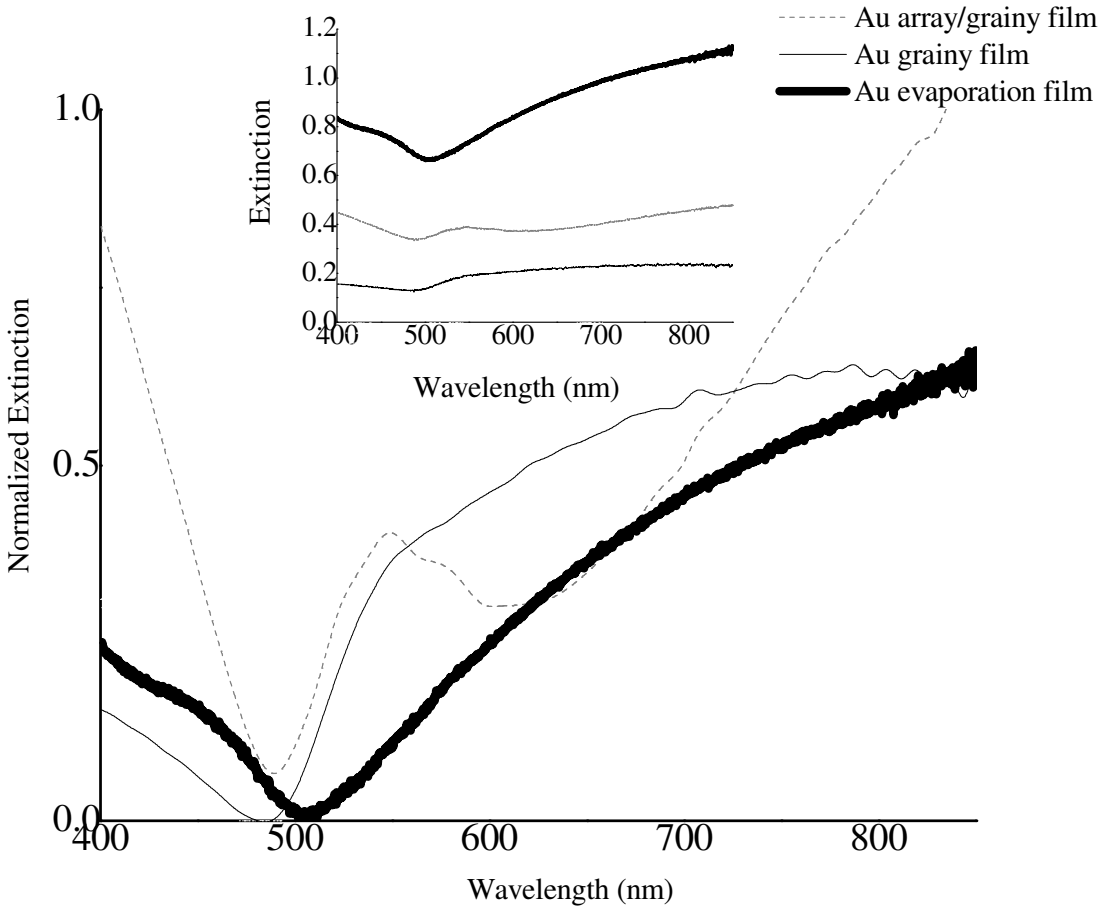

Fig. 2. Normalized transmission UV-vis spectra of the hexagonal array of the Au conglomerate nanocylinders on the Au grainy film (background), Au grainy film, and Au evaporated film. Inset are non-normalized spectra of the same three samples.

RSC Advances Accepted Manuscript

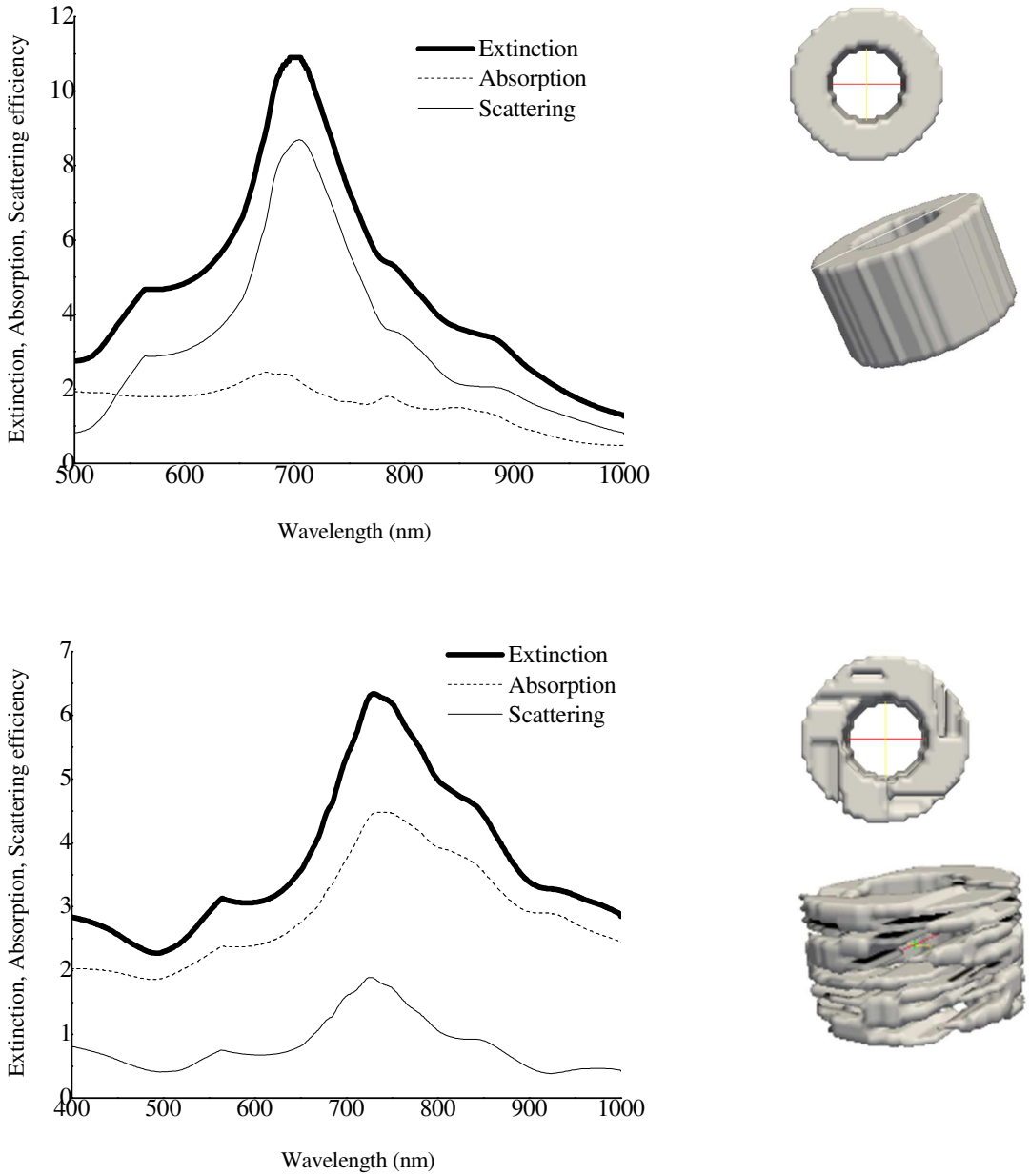

Fig. 3 Extinction, absorption, and scattering efficiency spectra of the solid cylinders (top) in comparison to grained cylinder shaped (bottom) by DDA simulations

RSC Advances Accepted Manuscript

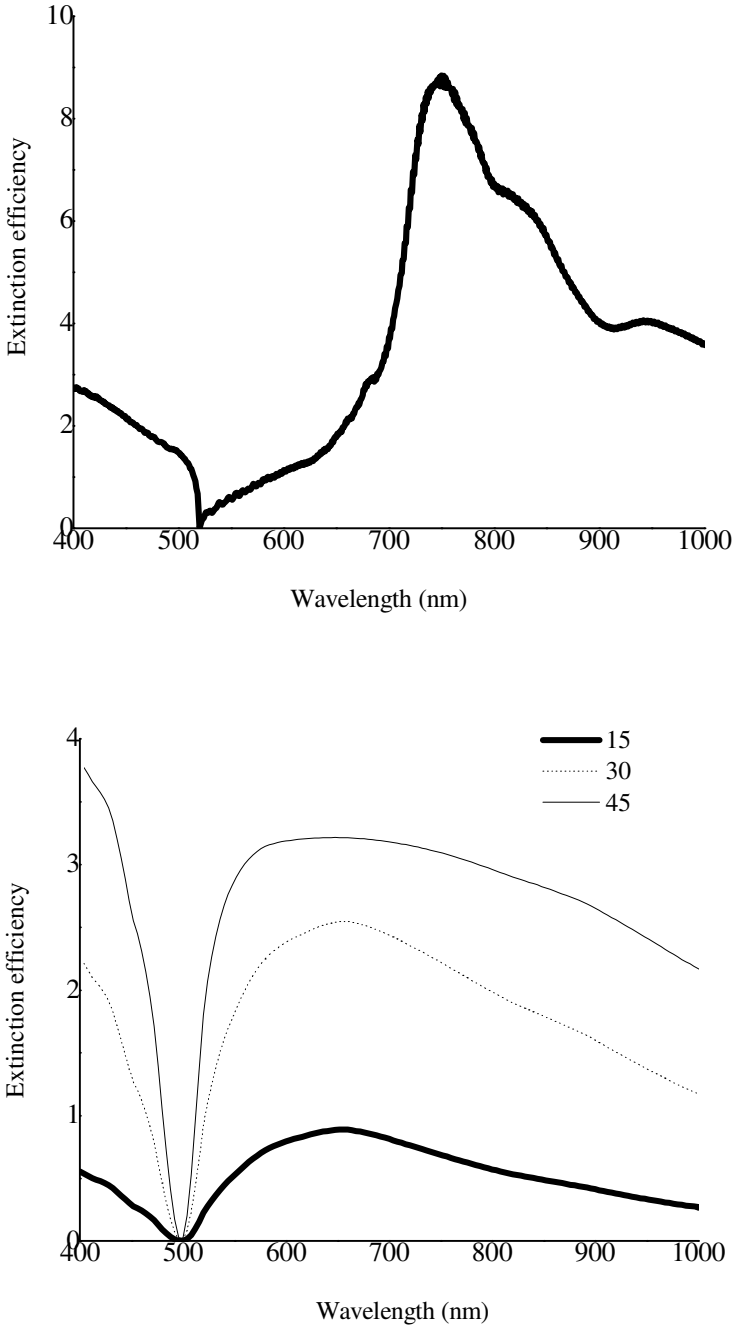

Fig. 4 Extinction efficiency spectra of the Au amorphous nanoconglomerated cylinders in the hexagonal array (top) by infinite coupled dipole (CDA) approximate simulations and grainy clusters, which consist of the 15, 30 and 45 of grains (bottom) in continuous films by discrete dipole approximation (DDA) simulations.

RSC Advances Accepted Manuscript

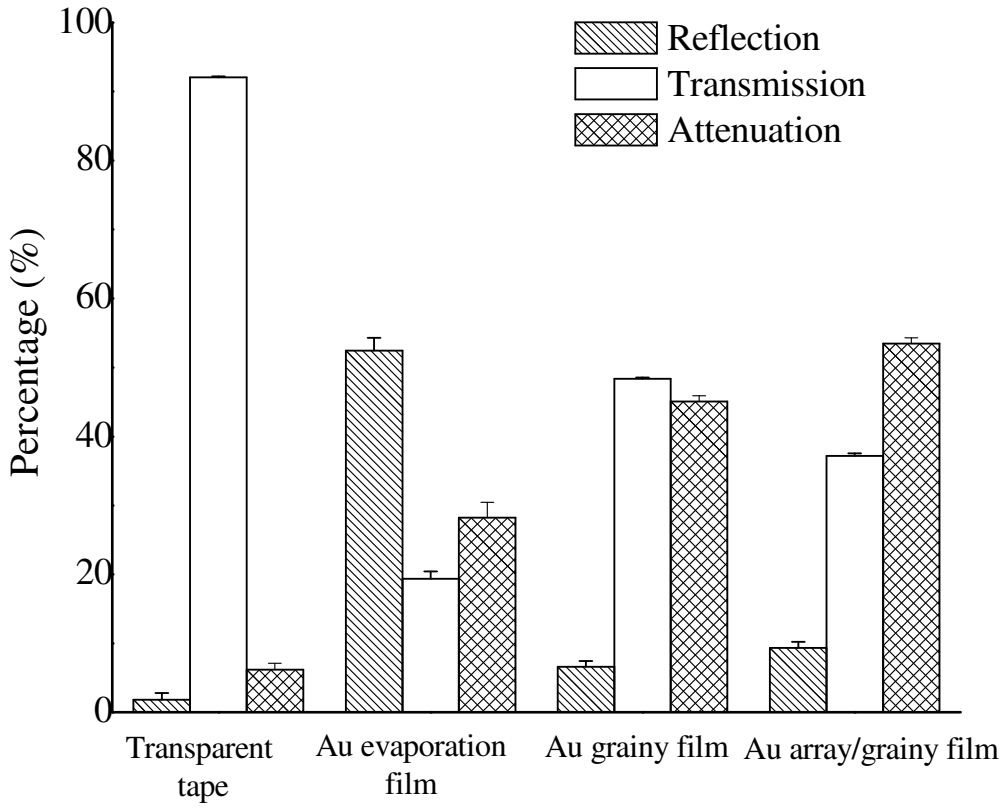

Fig. 5. Attenuation, transmission and reflection of the hexagonal array of the Au cylinder-nanoconglomerates on the Au grainy film (background), Au grainy film and Au evaporated film. The error bars correspond to standart deviation from the mean.

RSC Advances Accepted Manuscript

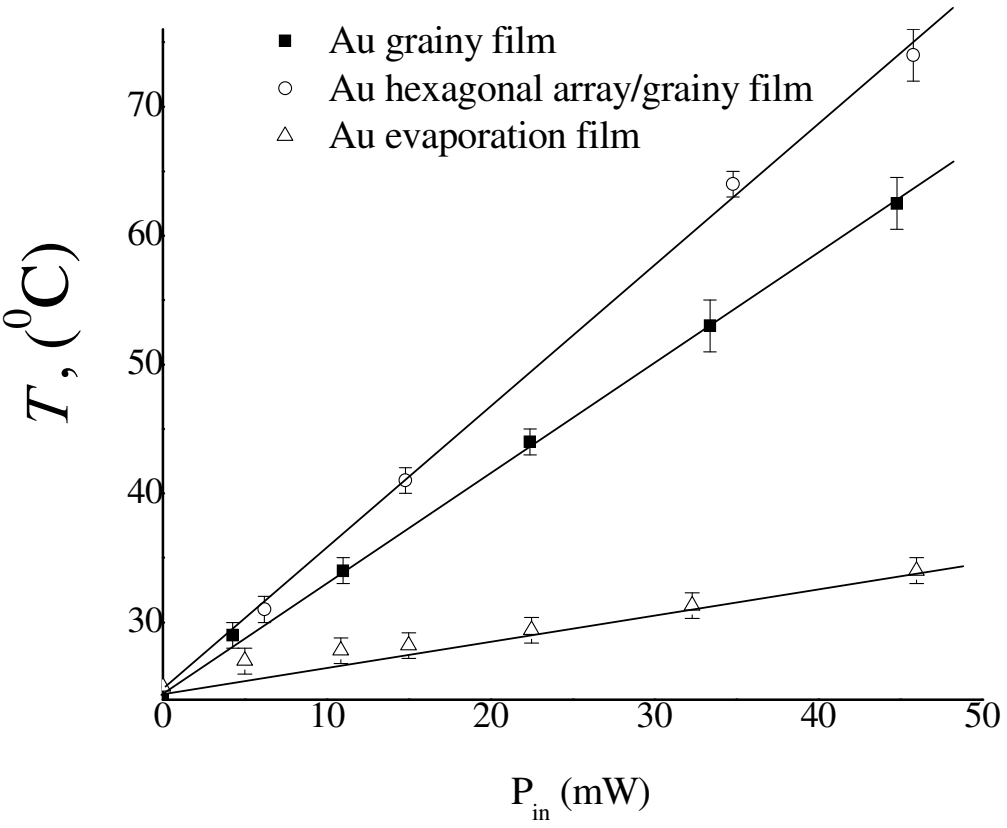

Fig. 6 The temperature versus the applied power (green laser) of the hexagonal array of the Au cylinder-nanoconglomerates on the Au grainy film (background), Au grainy film and Au evaporated film

RSC Advances Accepted Manuscript

References

1 A.G. Nikitin, T. Nguyen and H. Dallaporta, *Appl. Phys. Lett*., 2013, **102**, 22116.

2 N. Félidj, G. Laurent, J. Aubaed, G. Lévi, A. Hohenau, J. R. Krenn and F. R. Aussenegg, *J. Chem. Phys*., 2005, **123**, 221103.

3 Y. Chu, E. Schonbrun, T. Ang and K.B. Crozier,*Appl. Phys. Lett.,* 2008, **93**, 181108.

4 V.G. Kravetz, F. Schedin and A.N. Grigorenko, *Phys. Rev. Lett.,* 2008, **101**, 087403.

5 S. L. Teo, V. K. Liu, R. Marty, N. Large, E. A. Llado, A. Arbouet, C. Girard, J. Aizpurua, S. Tripathy and A. Mlayah, *Opt. Express*, 2010, **18**, 22271.

6 M. Alba, N. Pazor-Perez, B. Vaz, P. Formentin, M. Tebbe, M. A. Correa-Duarte, P. Granero, J. Ferre-Borrull, R. Alvarez, J. Pallares. A. Fery, A. R. De lera, l. F. Marsal and R. A. Alvarez-Puebla, *Angew. Chem. Int. Ed.,* 2013, **52**, 1.

7 S. Zou and G. C. Schatz, *Chem Phys Lett*., 2005, **403**, 62.

8 Y. Zhang, F. Wen, Y-R. Zhen, P. Nordlander and N. J. Halas, *PNAS*, 2013,**110**, 9215.

9 R.A. Pala, J. White, E. Barnard, J. Liu and M. L. Brongersma, *Adv. Mater*., 2009, **21**, 2504.

10 M. W. Knight, H. Sobhani, P. Nordlander and N. J. Halas, *Science*, 2011, **332**, 702.

11 D. Dejarnette, J. Norman and D.K.Roper, *Phys. Lett.*, 2012, **101**, 193104.

12 D. Dejarnette, D.K.Roper and B. Harbin, *JOSA B*., 2012, **29**, 88.

13 M. Lisunova, J. Norman, P. Blake, G. T. Forcherio, D. F. DeJarnette and D. K. Roper *J. Phys. D. Appl. Phys*., 2014, **46**, 241.

14 D.K. Roper, W.Ahn, B. Taylor and Y. D'Asen, *IEEE Sensors Journal*, 2010, **10**, 531.

15 W. J. Chen, T. Kan, Y. Ajiki, K. Matsumoto and I. Shimoyama, *PMMI meeting*, 2013.

16 Y. Ajiki, T. Kan, K. Matsumoto and I. Shimoyama. Papers transducers'11 Conference, Beijing, 2011.

17 M. R. Shcherbakov, P.P. Vabishchevich, V.V. Komarova, T.V. Dolgova, V. I. Panov, V.V. Moshchehalkov and A.A. Fedyanin, *Phys. Rev. Lett.*, 2012, **108**, 2539031.

18 P. Blake, J. Obermann, B. Harbin and D.K. Roper, *IEEE Sensors Journal*, 2011, **11**, 3332.

19 D. DeJarnette, G-G. Jang, P. Blake and D. K. Roper, in preparation.

20 T. Aihara, K. Nakagawa, M. Fukuhara, Y. L. Yu, K. Yamaguchi and M. Fukuda. *Appl. Phys. Lett*., 2011, **99**, 043111.

21 H. A. Atwater and A. Polman, *Nature Mater*., 2010, **9**, 205.

22 T. Ishi, J. Fujikata, K. Makita, T. Baba and K. Ohashi., *Jpn J. Appl. Phys*., 2005, **44**, 364.

23 D.K. Roper, W. Ahn and M. Hoepfner, *J. Phys Chem C*., 2007, **111**, 3636.

24 W. Ahn, and D.K. Roper, *J. Phys. Chem. C.*, 2008, **112**, 12214.

25 A. Russell, M. McKnight, A. Sharp, J. Hestekin, D. K. Roper, *J. Phys. Chem. C.*, 2010, **114**, 10132.

26 A.G. Russell, M. McKnight, J. Hestekin and D.K. Roper, *Langmuir,* 2011, **27**, 7799.

27 A.O. Govorov and H. Hugh, *Nanotoday,* 2007, **2**, 3.

28 A. O. Govorov, W. Zhang, T. Skeini, H. Richardson, J. Lee and N.A Kotov, *Nanoscale Res. Lett.*, 2006, **1**, 84.

29 S. Link, Z. L. Wang and M. A. El-Sayed, *J. Phys. Chem. B, 2000,***104***, 7867.*

30 K. Berry, A. Russell, P. Blake and D. K. Roper, *Nanotechnology,* 2012, **23**, 375703.

31 L. R. Hirsch, R. J. Stafford, J. A. Bankson, S. R. Sershen, R. E. Price, J. D. Hazle, N. J. Halas, and J. L. West, Proceedings of the Second Joint EMBS/BMES Conference, 2002**.**

32 X. Huang, P. K. Jain, I. H. El-Sayed and M. A. El-Sayed, *Lasers Med Sci*., 2008, **23**, 217.

RSC Advances Accepted Manuscript

[33] I. H. El-Sayed, X. Huang and M.A. El-Sayed, *Cancer Lett*, 2006, **239**, 129.
[34] X. Huang, P. K. Jain, I. H. El-Sayed and M.A. El-Sayed, *Photochem Photobiol*, 2006, **82**, 412.
[35] X. Huang, PI. H. El-Sayed and M.A. El-Sayed, *J Am Chem Soc*, 2006, **128**, 2115.
[36] A.O. Govorov and H. Hugh, *Nanotoday* 2007, **2**. 3.
[37] J.Hao, L.Zhou, M. Qiu. *Phys. Rev.* B, 2011, **83**, 165107.
[38] X. Chen, Y. Chen, M. Yan and M. Qiu, *ACSNanno*, 2012, **6**, 2550.
[39] W. Ahn, B. Taylor, Y. Dall-Asen, and D.K. Roper, *Langmuir,* 2008, **24**, 4174.
[40] W. Ahn and D.K. Roper. ACS National Meeting, Salt Lake City, 2009.
[41] G. G. Jang and D.K. Roper, *J. Phys. Chem C.*, 2009, **113**, 19228.
[42] G.-G. Jang, P. Blake, and D.K. Roper, *Langmuir*, 2013, **29**, 5476.
[43] X. Wei and D.K. Roper, *Journal of the Electrochemical Society*, 2014.
[44] A. Mooradian, *Phys. Rev. Lett*.. 1969, **22**, 185-187.
[45] J. H. Kim, and P. J. Moyer, *Opt. Expr.* 2006, **14**, 6595-6603.
[46] I. Doron-Mor, H. Cohen, Z. Barkay, A. Shanzer, A. Vaskevich, and I. Rubinstein, *Chem. A Euro. J*. 2005, **11**, 5555-5562.
[47] W. Ahn, B. Taylor, Y. Dall-Asen, and D.K. Roper, *Langmuir,* 2008, **24**, 4174.
[48] G. T. Boyd, Z. H.Yu, Y. R. Shen, *Phys. Re*V. *B* 1986, **33**, 7923-7936.
[49] P. Apell, R. Monreal, S. Lundquist, *Phys. Scr*. 1988, **38**, 174-179.
[50] P. B. Johnson, and R. W. Christy, *Phys. Rev. B*, 1972, **6**, 4370.
[51] M. Hu, J. Chen, Z.-Y. Li, L. Au, G. V. Hartland, X. Li, M. Marqueze and Y. Xia, *Chem Soc Rev.,* 2006, **35**, 1084.
[52] M. A. Mahmoud, and M. A. El-Sayed, J. Phys. Chem. B, 2013, 117, 4468-4477.
[53] Yurista C L and Friesem A A *Appl. Phys. Lett*., 2000, **77** 1596.
[54] G. T. Forcherio and D. K. Roper, *Appl. Optics*, 2013, **52**, 6417.
[55] J. Cai, J. Ye, S. Chen, X. Zhao, D. Zhang, S. Chen, Y. Ma, S. Jin, and L. Qi*, Energy Environ. Sci.* 2012, **5**, 7575.
[56] H. Liu, Q. Zhao, H. Zhou, J. Ding, D. Zhang, H. Zhu and T. Fan, *PCCP,* 2011, **13**, 10872.
[57] J. Dunklin, G. Forcherio, K. Berry, and D.K. Roper, *ACS Appl. Mat. Interf.* 2013, **5**, 8847.
[58] P. K. Jain, K. S. Lee, I. H. El-Sayed and M. A. El-Sayed, *J Phys Chem B*, 2006, **110**, 7238.
[59] V. Kotaidis, C. Dahmen, G. von Plessen, F. Springer and A. Plech, J. Chem. Phys. , 2006, **124**, 184702.
[60] J.Hao, L.Zhou and M. Qiu. *Phys. Rev.* B, 2011, **83**, 165107.
[61] X. Chen, Y. Chen, M. Yan and M. Qiu, *ACSNanno*, 2012, **6**, 2550.
[62] N. Zeng andA. B Murphy. *Nanotechnology*, 2009, **20**, 375.
[63] M. T. Carlson, A. Khan and H. H. Richardson, *Nano Lett.,* 2011, **11**, 1061
[64] M. Perner, P. Bost, G. von Plessen, J. Feldmann, U. Becker, M. Mennig and H.Schmidt, *Phys. ReŠ. Lett*., 1997, **78**, 2192.
[65] S. Link, C. Burda, Z. L. Wang and M. A. El-Sayed, *J. Chem. Phys*., 1999, **111**, 1255.
[66] N. W. Ashcroft, N. D. Mermin, *in Solid State Physics*, Philadelphia, Pennsylvania: Saunders College, 1976.
[67] J. I. Kim, D.-R. Jung, J. Kim, C. Nahm, S. Byun, S. Lee and B. Park, *Solid State Communications*. 2012, **152**, 1767.
[68] B. J. Lawrie, R. F. Haglund Jr, R. Mu. *Opt. Express*, 2009, **17**, 2565.
[69] D. Zhang, H. Ushita, P. Wang, C. Park, R. Murakami, S.-C. Yang and X. Song, *Condensed Matter*, DOI:10. 1063/1.4819476.
[70] M. Lisunova, M. Mahmoud, N. Holland, Z. Combs, M. A. El-Sayed and V. V. Tsukruk. *J Mater. Chem*. 2012, **22**, 16745.

RSC Advances Accepted Manuscript

[71] V. H. Chu, E. Fort, T. H. L. Nghiem and H. N. Tran, *Adv. Nat. Sci.: Nanosci. Nanotechnol*., 2011, **2**, 045010.
[72] P. Blake, W. Ahn and D. K. Roper, *AIChE Annual Meeting,* Nashville, 2009.
[73] G. T. Forcherio and D. K. Roper, *Appl. Optics*, 2013, **52**, 6417.
[74] B. T. Draine and P. J. Flatau, *J. Opt. Soc. Am. A,* 1994, **11**, 1491.
[75] P. J. Flatau and B. T. Draine, *Optics Express,* 2012, **20**, 1247.
[76] P. B. Johnson and R. W. Christy, *Phys. Rev. B*, 1972, **57,** 783.
[77] J. Normnan, D. Dejarnette and D., Roper, D.K., *J Phys Chem C*, 2014, DOI:10.1021/jp408706j.

RSC Advances Accepted Manuscript